J Nanopart Res (2013) 15:1500
DOI 10.1007/s11051-013-1500-1

RESEARCH PAPER

EELS compositional and valence mapping in iron fluoride–carbon nanocomposites

Jafar F. Al-Sharab · James Bentley · Fadwa Badway · Glenn G. Amatucci · Frederic Cosandey

Received: 29 November 2012 / Accepted: 9 February 2013 / Published online: 12 March 2013

Abstract Iron fluoride–carbon nanocomposites (FeF_2–C and FeF_3–C) are newly developed materials for positive electrodes in Li–ion batteries. These new composites represent high-capacity and reversible conversion electrode materials with capacity close to theoretical value and four times that of lithium cobalt oxide; the most widely used compounds as positive electrode. In this paper, we report detailed chemical and structural analysis of FeF_2–C nanocomposite electrode at different discharge states. The FeF_2–C nanocomposite was prepared by high-energy ball milling at ambient conditions and further processed in helium environment. The as synthesized electrode consists of FeF_2 nanodomains with crystallite size ranging from 2 to 18 nm in an amorphous carbon matrix. The electrode material was analyzed by the electron energy loss spectroscopy (EELS) compositional imaging with nanometer resolution, and selected area electron diffraction (SAED) at 36 %, 75 %, and fully discharged states. The high-resolution EELS elemental maps and intensity line profiles of Fe and F were obtained to investigate phase transformation during discharge. Valence maps of Fe were also produced based on the Fe L_3/L_2 white line intensity ratios. The 2-nanometer scale EELS elemental maps reveal that Fe in the as processed electrode consists of a mixed valence states (2^+ and 3^+). The discharged samples at 36 and 75 % demonstrate compositional modulation with F-rich and F-depleted areas with the fully discharged material consisting of nanoscale regions of LiF and Fe in agreement with the cathodic conversion reaction.

Keywords FeF_2–C and FeF_3–C nanocomposites · Radiation damage in FeF_2 · EELS valence mapping · EELS compositional mapping · High-capacity iron fluoride nanocomposites · Reversible conversion lithium ion batteries

Electronic supplementary material The online version of this article (doi:10.1007/s11051-013-1500-1) contains supplementary material, which is available to authorized users.

Special Issue Editors: Juan Manuel Rojo, Vasileios Koutsos

This article is part of the topical collection on Nanostructured Materials 2012

J. F. Al-Sharab · F. Badway · G. G. Amatucci · F. Cosandey
Department of Materials Science and Engineering, Rutgers, The State University of New Jersey, Piscataway, NJ 08904, USA

Present Address:
J. F. Al-Sharab (✉)
Department of Mechanical & Aerospace Engineering, Polytechnic Institute of New York University (NYU-Poly), Six MetroTech Center, RH 511, Brooklyn, NY 11201, USA
e-mail: jafarhan@rci.rutgers.edu

J. Bentley
Materials Science and Technology Division, Oak Ridge National Laboratory, Oak Ridge, TN 37831-6064, USA

Introduction

The energy density of Li–ion batteries is directly related to the capacity of positive and negative electrodes (Badway et al. 2003a; Badway et al. 2003b; Nazri 2003a; Plitz et al. 2005; Dupin et al. 2001; Chen et al. 2011). The current positive electrode such as $LiCoO_2$ uses the intercalation reactions to obtain high-energy Li–ion batteries. Lithium cobalt oxides are the most widely used compounds in intercalation due to their good capacity, cycle life, and storage performance (Amatucci et al. 1996; Wan et al. 1999; Chen et al. 2002; Badway et al. 2003a; Markovsky et al. 2004; Kosova et al. 2003; Nazri 2004; Gabrisch et al. 2005). However, the capacity of this layered structure is limited due to the dependency of Li intercalation on vacancy concentration (Shao-Horn et al. 2003) and incomplete reversibility at high degrees of delithiation/specific capacity (Cosandey et al. 2005; Cosandey et al. 2006). In addition, almost all intercalation material reversibility is limited to one electron per *3d* transition-metal ion. Therefore, there is a need for a new generation of positive electrodes with higher capacity. A pathway toward lithium batteries with a significant improvement in capacity can be obtained with transition-metal materials, which favors high-oxidation state and utilize all oxidation states according to the following reaction.

$$n\mathrm{Li}^{+} + n\mathrm{e}^{-} + \mathrm{Me}^{n+}\mathrm{X}_{n} \leftrightarrow n\mathrm{LiX} + \mathrm{Me}^{0}, \quad (1)$$

where Me is transition metal.

A few researchers have explored new routes that have led to promising results (Arai et al. 1997; Poizot et al. 2000). Recently, carbon metal fluoride nanocomposites (CMFNC) such as FeF_3–C and FeF_2–C as new materials for positive electrodes in Li–ion batteries (Badway et al. 2003a; Badway et al. 2003a–c; Plitz et al. 2005) have been introduced. The FeF_2–C material demonstrated excellent performance with energy capacity 4 times that of classical Li_xC_6–$Li_{1-x}CoO_2$ system with full reversibility (Badway et al. 2003a; Plitz et al. 2005). Although bulk FeF_2 is an insulator material, excellent properties were obtained by the synthesis of FeF_2–C nanocomposites consisting of FeF_2 nanostructured domains in a high-conductivity carbon matrix (Badway et al. 2003a; Plitz et al. 2005). The electrochemical reaction in a charging/discharging reaction can be described as follows:

$$2\mathrm{Li}^{+} + 2\mathrm{e}^{-} + \mathrm{Fe}^{2+}\mathrm{F}_2 \leftrightarrow 2\mathrm{LiF} + \mathrm{Fe}^{0} \quad (2)$$

Based on this reaction, the calculated theoretical specific capacity is 546 mAh/g while the best experimental value was 500 mAh/g (Badway et al. 2003a; Plitz et al. 2005). At the present time, the exact reaction path mechanisms and phase transformation which accompany the charging and discharging processes are still not fully understood. There is therefore a need to obtain information on chemistry, structure, and electronic properties at the nanometer scale. In this regard, high-resolution EELS (HR-EELS) spectroscopy is a powerful technique which can provide nanometer scale chemical composition information (Reimer 1995; Egerton 1996) as well as chemical environment of the exited atoms (Saifullah et al. 1999). The chemical composition can be measured directly from core-loss edges which result from the transition of core electrons to unoccupied states in the conduction band (Garvie et al. 1994), while valence state of Fe and other transition elements can be determined from the ratio of white lines, L_3 and L_2 intensities and their energy (Saifullah et al. 1999; Cosandey et al. 2005; Cosandey et al. 2006).

In a previous study (Cosandey et al. 2005; Cosandey et al. 2006), we have investigated FeF_2–C and FeF_3–C nano composites electrodes at different discharged and recharged values. These samples have been characterized using high-resolution TEM (HRTEM), selected area electron diffraction (SAED) and electron energy loss spectroscopy (EELS) (Cosandey et al. 2005; Cosandey et al. 2006). However, the analyses from our previous EELS study were collected from individual raster areas 30 by 30 nm in size giving rise to only average information as the FeF_2 nano domains are in the range of 2–30 nm. At the present time, there is a need to study this materials on a scale smaller than the nano domains to provide a deeper insight into the lithiation reaction. Understanding of the special distribution of the converted phases is paramount to gaining an insight on both the ionic and electronic diffusion.

Therefore, in order to gain further insight into the structural and chemical changes occurring during discharge, we have studied FeF_2–C nanocomposite electrodes at various stages of discharge (36 %, 75 %, and fully discharged) by means of 2D STEM-EELS compositional and Fe-valence mapping. Because the starting material FeF_2 and the transformed material

after discharge (LiF and Fe) have similar EELS edges, an analysis of elemental edges for each compound is presented showing the characteristic EELS signal that allow identification of specific compounds.

In addition, as fluoride compounds are electron beam sensitive, a time-dependent EELS analysis of FeF_2 is presented to understand the decomposition kinetics and F loss during EELS analysis and to determine the optimal STEM experimental parameters in terms of beam size and electron dose.

Experimental procedure

The carbon metal fluoride nanocomposites (CMNC) were fabricated in He by high-energy ball milling. In this technique, stoichiometric mixtures of FeF_2 (Alfa) and activated carbon (15 wt%), ASupra (Norit) were placed inside a hardened-steel milling cell along with hardened-steel media. All cell assemblies were performed in a He-filled glove box. More details on the synthesis of the FeF_2–C nanocomposites, preparation of the cathodes and testing procedures can be found elsewhere (Badway et al. 2003a; Plitz et al. 2005).

The TEM samples were prepared from the disassembled electrodes by dispersing the milled powder in "trichlorotrifluoroethane" and releasing a few drops of the liquid on an amorphous, "lacey" carbon film supported on copper grid. Then, the mixture was allowed to dry leaving behind particles dispersed on the TEM grid. All preparations were accomplished in an anhydrous He atmosphere. The grids were sealed under helium and transferred to the TEM chamber. The final transfer to the TEM chamber consisted of less than 30 s exposure to ambient atmosphere.

HR-EELS spectrum imaging was conducted using a Philips CM200 FEG TEM equipped with Gatan imaging filter (GIF) operating in STEM-mode at 197 kV. All spectra were acquired and processed with Emispec Vision and also exported for further analysis with Gatan EL/P software. Initial data were taken with an in-focus STEM probe of $\sim$1.0 nm at FWHM and 1.2 nA probe current. However, the beam intensity was too high causing a severe loss of fluorine. This problem was minimized using an under-focused STEM probe with a diameter of $\sim$2 nm. This assured a dose rate of less than 5×10^3 Ccm^{-2} s^{-1}. With this setup, an energy resolution of 1 eV was routinely obtained using a collection half angle beta of 10 mrad, convergence angle alpha of 8 mrad, and the EELS spectra were collected with 0.1 eV dispersion per channel. All EELS spectra were automatically corrected for sample drift. The optimum exposure time with statistically significant counts and minimum damage was found to be 10 readout in 10 ms for the low-loss spectra while for the core-loss the exposure time was increased to 0.1 s leaving the number of read out unchanged (i.e., 10 readouts/second).

A three-window polynomial background-fit was used to remove the background and extract the intensity of the Fe–L_2 and Fe–L_3 white lines. The Fe L_3/L_2 white line intensity (WLI) ratios were determined by taking the ratio of the sum of intensities of the L_3 and L_2 white lines. For the Fe L_3 and L_2 white lines, the width of the energy window was 9 eV. For the F(K) an Li(K) edges, a conventional inverse power-law background fit and an energy window of 15 eV were used to obtain the F–K edge intensity. In view of the beam sensitivity of the material, the corresponding zero-loss peak was not collected and therefore, these spectra were not corrected for plural scattering.

Results

A typical voltage curve for lithiated FeF_2–C cell cycled between 1.5 and 4.5 V is shown in Fig. 1 for a discharge rate of 7.5 mA/g. During the first discharge, a plateau-like feature is observed at approximately 3 V for the first 6 h or so. This could be attributed to a small degree of Fe^{3+} in the starting material, however no evidence for its presence could be given by XRD.

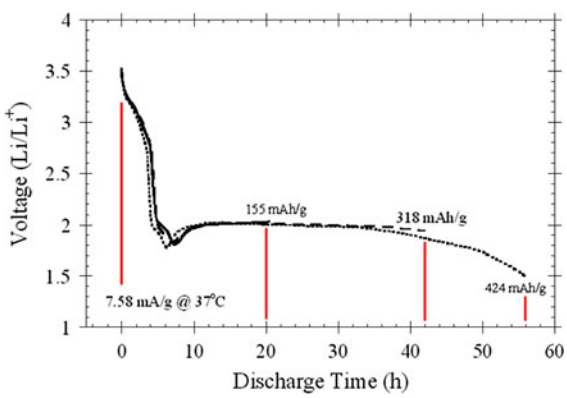

Fig. 1 Voltage discharge profile for the FeF_2–C nanocomposite electrode at 37 °C and for a discharged rate of 7.5 mA/g. The *vertical red lines* indicate the samples studied. (Color figure online)

This observation will be investigated in further detail below. The second plateau at approximately 2 V initiates with a bit of over potential which arises with the nucleation of the 2LiF + Fe discharge process. As per theory, the conversion reaction proceeds until 56 h (424 mAh/g of composite, which is equivalent to 500 mAh/g of FeF_2). Samples which were investigated by STEM-EELS are marked in Fig. 1 with vertical lines on the voltage profile corresponding to discharge times of 20 (152 mAh/g), 42 (318 mAh/g) and 56 h (424 mAh/g; fully discharged).

TEM characterization

Phase identification process from EELS spectra

Upon total discharge, LiF and Fe are expected to be the final product of the initial FeF_2 positive electrode. As the F–K and Fe–$L_{2/3}$ core-loss signal will always be present regardless of the discharge state, there will not be sufficient information to assess whether the elements are in the form of unreacted FeF_2 or discharge reacted products LiF + Fe. Therefore, it is essential to collect the low-loss spectra to detect in addition to F, the simultaneous presence of Li. Moreover, identification of oxidation state of Fe in either $Fe^{2+}F_2$, $Fe^{3+}OF$, $Fe^{3+}F_3$ or metallic Fe^o can be obtained from the energy position of the L_3 and L_2 white lines and from their intensity ratio (Egerton, 1996). In a previous study (Cosandey et al. 2006), we have been able to uniquely identify $Fe^{2+}F_2$ from $Fe^{3+}F_3$ from the 1.5 eV decrease in the Fe–L_3 line energy. The Fe–L_3 line energies in $Fe^{2+}F$ and Fe^o are almost the same and cannot be used for phase identification. However, a unique Fe^{2+} versus Fe^o oxidation state determination can be obtained from the decrease in L_3/L_2 line intensity ratio. Exact value in Fe L_3/L_2 intensity ratio between various Fe oxidation states is strongly dependent on EELS acquisition parameters and methodology to extract the L_3 and L_2 white line intensities (Egerton, 1996). However, regardless of the specific methodology, the Fe L_3/L_2 intensity ratio decreases with reduction in oxidation state from Fe^{3+} to Fe^{2+} and Fe^o. Examples of low-loss and core-loss spectra of as synthesized FeF_2–C electrode material are shown in Fig. 2a, b respectively. The Fe–M_{23} edge is observed in Fig. 2a with peak intensity at 60 eV. On the other hand, F–K (693.4 eV), Fe–L_3 (708.7 eV), and Fe–L_2 (721.5 eV) of FeF_2 are visible in Fig. 2b (curve *b*1).

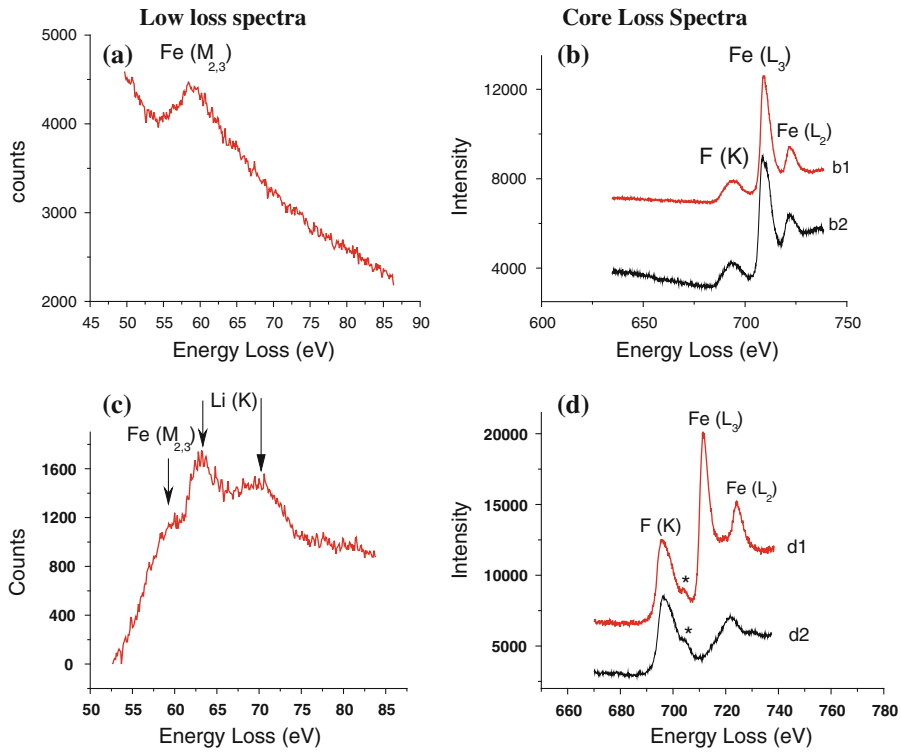

Fig. 2 Phase identification process used in EELS analysis. **a** Low-loss, and **b** core-loss spectra of FeF_2. Curve *b*1 is from a region with homogenous di-valence state, Fe^{2+}, while curve *b*2 is from an area containing mixed di- and tri-valence states, Fe^{+2} and Fe^{+3}. **c** Low-loss with Li–K and Fe–$M_{2,3}$ signals, and **d** core-loss spectra with Fe–$L_{2,3}$ and F–K signals (curve *d*1) of an area containing mixed LiF and Fe phases. The standard F–K EELS signal from LiF with *unique post F–K peak* is also shown in Fig. 2d, curve *d*2

In Fig. 2b (curve *b*2) a broadening/splitting in L_3 white line is indicative of co-existence of multiple valence states of Fe (Fe^{2+}, and Fe^{3+}). In other words, EELS has the capability of differentiating between FeF_2 (curve b1) and the coexistence of multiple valence states (2^+ and 3^+) such as between FeF_2 and FeF_3 or FeOF (curve b2). This Fe L_3/L_2 ratio method will be used later for quantitative analysis of valence state mapping.

The low-loss and core-loss spectra from a fully discharged sample are shown in Fig. 2c, d (curve *d*1) respectively. The F–K core-loss from LiF standard is shown in Fig. 2d. In addition to the presence of the Li–K edge, identification of the LiF phase can be based also on a unique feature of the F–K edge with *post F–K peak* located ~5 eV to the right of the main F–K edge located at around 704 eV. This *post F–K peak* is marked with an asterisk (*) in Fig. 2d (curve *d*2), taken from the standard LiF compound. Therefore, in the spectra shown in Fig. 2d (curve *d*1) the presence of *post F–K peak* together with Li–K signal are indications that F and Li are combined as LiF despite the presence of Fe in the EELS spectra in Fig. 2c, d. The above procedure was followed to analyze our spectrum images and to uniquely identify all phases in our EELS compositional maps.

Time series and radiation damage experiment

Owing to the high sensitivity of fluorine compounds to electron beam irradiation, the impact of beam damage on measured EELS data was determined from drift-corrected time series experiments. These experiments were essential because they allow investigating the effect of electron beam damage on phase decomposition, chemistry, and bonding with accurate estimation necessary for quantitative analysis. Therefore, in each damage experiment, the beam remained stationary for 50 s and the EELS spectra were recorded every second at a dose rate of 1.5×10^5 C/cm^2/s. Figure 3a is a time series plot of the fluorine F–K and iron white lines Fe–L_3 and Fe–L_2 intensities recorded as a function of time. Figure 3b shows the relative intensities of Fe–L_3 to Fe–L_2 and F–K to Fe–L_3 (Fe–L_3/Fe–L_3 and Fe–L_3/Fe–L_2) of the EELS spectra collected in Fig. 3a. Although both F and Fe–L_3/L_2 ratios decrease exponentially with time, the Fe–L_3/Fe–L_2 represent the reduction in oxidation states from Fe^{2+} to Fe^o, while the F–K/Fe–L_3 represent a fluorine loss phenomenon. The plot also shows the fluorine content initially decreases at rate of

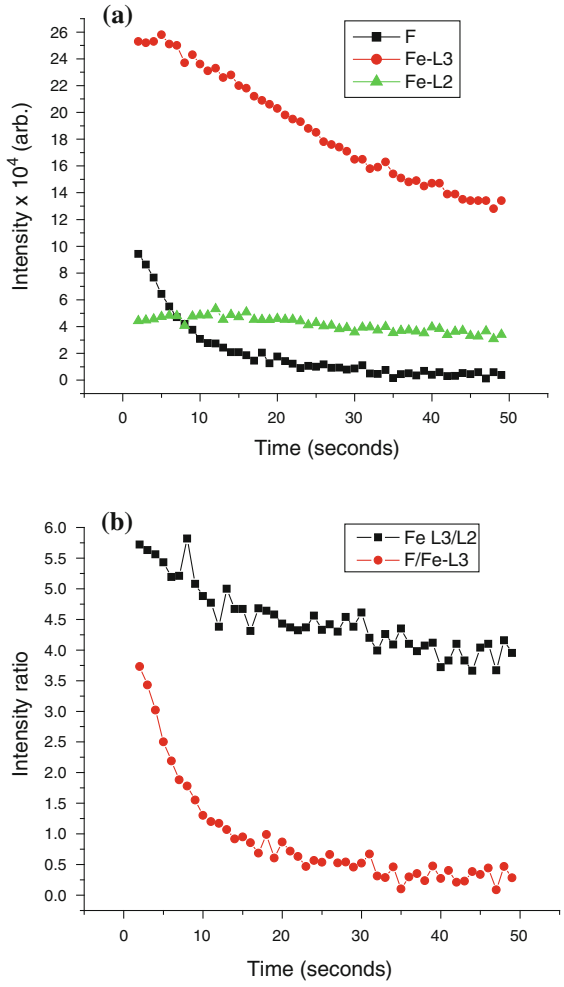

Fig. 3 Radiation damage experiment in FeF_2–C nanocomposites. **a** Time series experiment of F–K, Fe–L_3, and Fe–L_2 EELS peak intensities taken with a stationary electron beam, and **b** Fe–L_3/L_2 and F–K/Fe–L_3 intensity ratios of data in **a**

8 % per second which is ~4 times faster than the decrease in the Fe–L_3/L_2 intensity ratio. After ~35 s which is equivalent to a total dose of 1.3×10^6 C/cm^2, the fluorine is completely depleted. This is obviously an indication that the initial FeF_2 structure will undergo transformation into FeF_{2-x} accompanied with valence state reduction ($Fe^{2+} \rightarrow Fe^0$) and after ~35 s the remaining material will be metallic Fe. The measured decrease of the Fe L_3/L_2 ratio from 5.8 to 3.8 upon the reduction in valence state from Fe^{2+} to Fe^o will be used later to determine the Fe valence of various discharge samples.

As mentioned above the fluorine content with 1 nm probe and a dose rate of 1.5×10^5 C/cm^2/s decreases

Table 1 Probe conditions with corresponding dose rate and fluorine loss in STEM-mode

Probe condition (size (FWHM), current)	Mode	Dose (C/cm^2/s)	Fluorine loss in 1 s
1 nm, 1.2 nA	Spot	1.5×10^5	8 %
2 nm, 1.2 nA	Spot	3.8×10^4	2 %

rapidly at rate of 8 % per second. Therefore, in order to collect maps and individual spectra, we used a 2 nm de-focused beam conditions corresponding to a dose rate of 3.8×10^4 C/cm^{2}s. Under these experimental conditions, the F loss is less than 2 % per second. Table 1 summarizes the investigated probe conditions with their dose rate and resulting fluorine loss.

HR-EELS maps of the as-prepared FeF_2–C nanocomposite electrode

A HRTEM lattice image, selected area electron diffraction (SAED) pattern, and corresponding dark field image of the as-prepared FeF_2–C nanocomposite electrode are shown in Fig. 4. The lattice fringes in the HRTEM image and *d*-spacings from SAED confirm the tetragonal crystal structure of FeF_2 with *P42mnm* space group. Crystallite size of the as synthesized material is ranging from 2 to 18 nm as can be observed from the nanodomains in the HRTEM, Fig. 4a, and from the dark field image in Fig. 4c.

A STEM image of the as-prepared FeF_2–C (unreacted) FeF_2–C electrode and corresponding compositional EELS maps are shown in Fig. 5. The Fe–L_3 white line intensity map is shown in Fig. 5b. The white line intensity ratio map of Fe (Fe–L_3 divided by Fe–L_2) is displayed in Fig. 5c. The intensity of the F–K map and the intensity ratio of fluorine to iron (F–K divided by Fe–L_3) are displayed in Fig. 5d, e respectively. The average Fe L_3/L_2 ratio from map in Fig. 5c was calculated to be 4.8 with standard deviation of 0.5 corresponding to the expected Fe^{2+} oxidation state. Some regions however, show higher Fe–L_3/L_2 intensity ratio in the range of 5.5–6.6 indicating a higher Fe^{3+} valence state. These regions correspond to tri valence state of Fe (Fe^{3+}) in addition to the di valence state (Fe^{2+}), as can easily be recognized from the Fe L_3/L_2 map as they appear in yellow color. Typical spectra from these two areas are shown in Fig. 5f, curves *f*1 and *f*2. The presence of mixed Fe^{+2} and Fe^{+3} valence states can be seen also in curve *f*2 from the presence of two overlapping L_3 edges from the presence of two valence states. The fraction of area with Fe^{3+} oxidation state based on the relative yellow area to the total area is about 4 %. The presence of the Fe^{3+}-based compounds (FeF_3 or FeOF) can be related to an induced oxidation while high-energy milling to create nanodomains of FeF_3, or an oxidation process caused by reaction with residual oxygen to form FeOF, or even the formation of Fe^{3+} within the pure fluoride rutile structure manifested as areas of trirutile. Iron in Fe^{+3} valence state will provide an extra charge during the total reduction to pure iron (Fe^0). However, reduction of FeOF or FeF_3 during the discharging process will occur in a two-step reaction ($Fe^{3+} \rightarrow Fe^{2+} \rightarrow Fe^0$) process instead of one-step reaction ($Fe^{2+} \rightarrow Fe^0$).

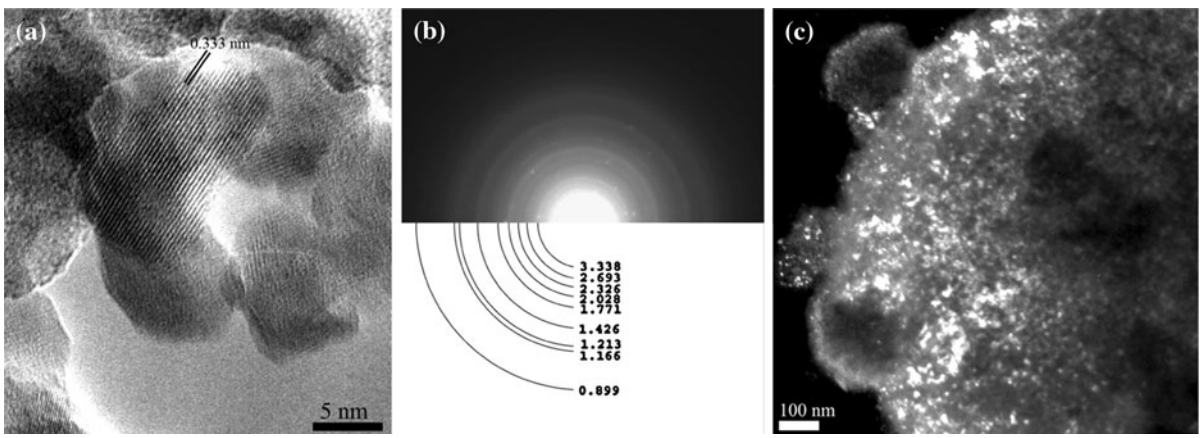

Fig. 4 **a** High-resolution TEM image. **b** Selected area electron diffraction (SAED), and **c** dark field image of the as synthesized FeF_2–C electrode

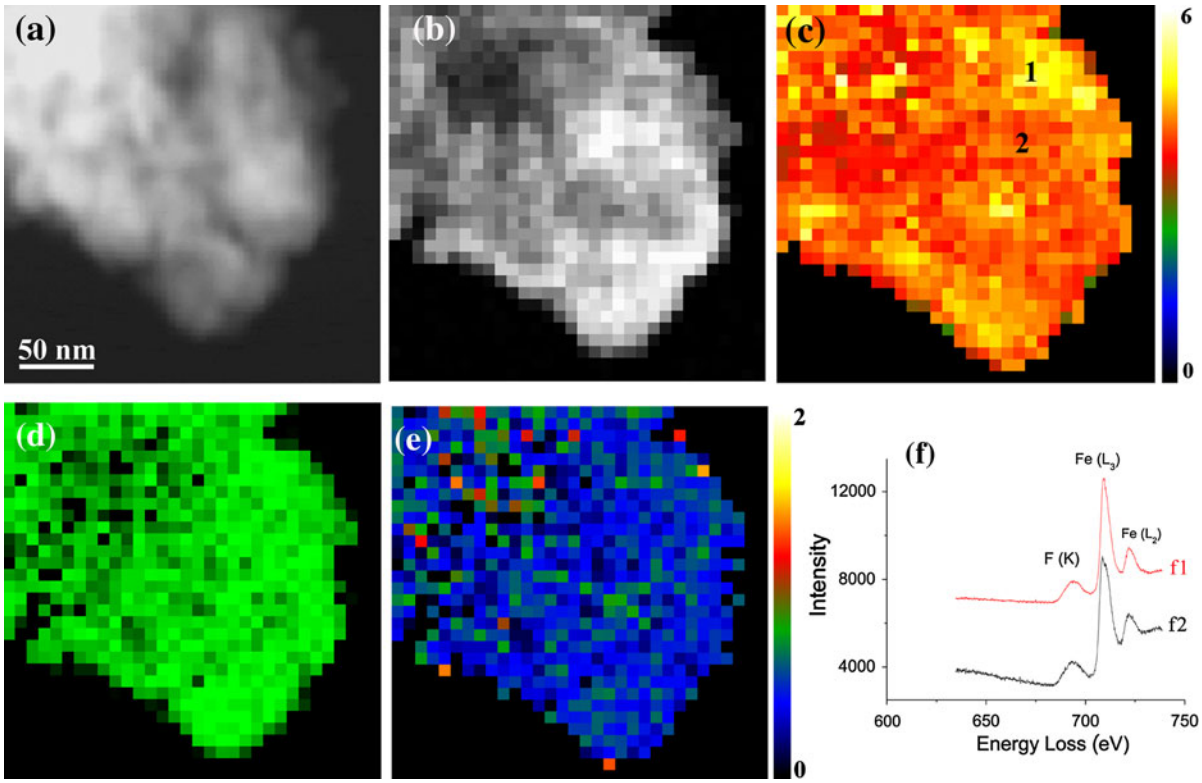

Fig. 5 EELS analysis of the as synthesized FeF_2–C nanocomposite electrode. **a** STEM image, **b** Fe–L_3 intensity map, **c** Fe L_3/L_2 intensity ratio map, **d** F–K intensity map, **e** F–K/Fe–L_3 ratio map, and **f** Individual EELS spectrum taken from regions *1* and *2* marked in **c** (each map is 256 by 256 nm^2)

The fluorine map, Fig. 5c, shows almost homogenous intensity across the mapped area except for few spots, which are fluorine depleted. The F/Fe–L_3 intensity ratio image also shows uniform intensity with an average of 0.46 and standard deviation of 0.1 corresponding to Fe^{2+} oxidation state. Low-loss spectra from this region show only core signal from $Fe_{M2,3}$ indicative of the presence of only FeF_2.

Line intensity profiles of electrodes discharged for 20, 42, and 56 h (fully discharged)

In order to further investigate the phase decomposition and structural inhomogeneity during discharge, EELS line profiles were collected from samples discharged for 20, 42, and 56 h (fully discharged). Thirty-two data points were collected along a line of 64 nm length with 5 nm spacing between the points. At each data point a full spectra of low-loss (zero-100 eV) and core-loss regions (650–750 eV) were collected. Furthermore, the Fe–L_3, Fe–L_2, and F–K intensity were obtained after background removal. Typical spectra from the sample discharged for 20 h showing partial transformed into LiF and Fe are displayed in Fig. 6. In the core-loss spectra, both F and Fe are present, however, only $Fe_{M2,3}$ edge is present in the low-loss region without any Li signal. Therefore, this is a FeF_2 compound with an energy line of the Fe–L_3 located at 709.0 eV consistent with the location of Fe^{2+} energy position. Figure 7 compares the intensity profiles of F–K/Fe–L_3 for samples discharged for 20, 42, and 56 h (fully discharged). All samples show variations in the F to Fe relative intensities. This variation can be related for two reasons. First, it can be caused by the variation in the Fe and F contents due to the reaction with Li ions and second due to the presence of the conductive carbon matrix. Taking these two factors into consideration, a modulation in the Fe L_3/L_2 ratio with period of $\sim$5 nm for the 20 h and 10 nm for the 42 h samples are measured. Fully discharged sample, however, showed large modulation ($\sim$16 nm) with respect to the partially discharged electrodes. This

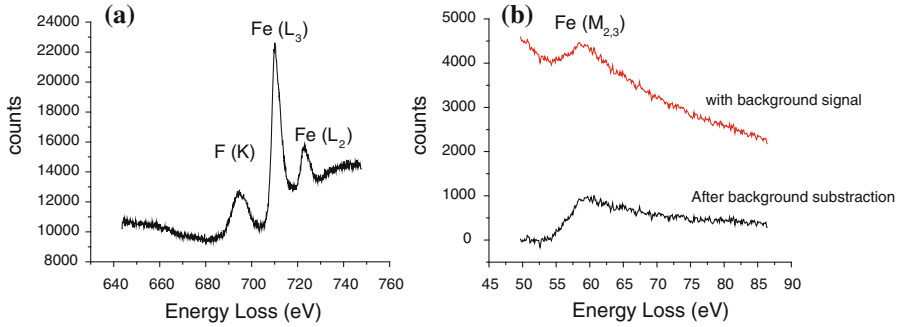

Fig. 6 EELS spectra from FeF_2–C nanocomposite electrode discharged for 20 h. **a** Core-loss spectra with F and Fe signals, and **b** low-loss spectra where the Fe–$M_{2,3}$ and Li–K are located

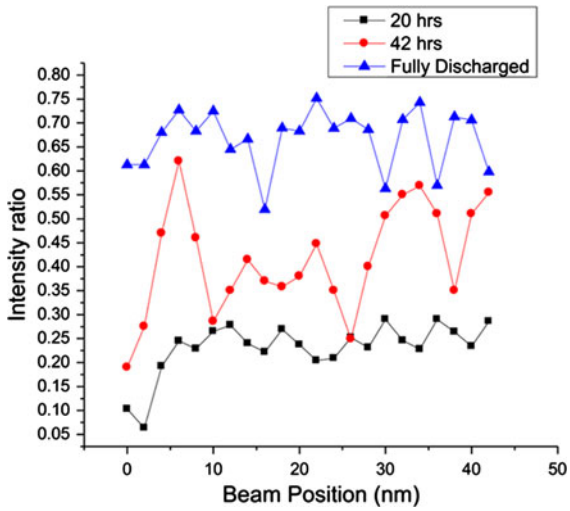

Fig. 7 Line profiles of F–K/Fe–L_3 intensity ratios of the FeF_2–C electrode discharged for 20, 42, and 56 h (fully discharged)

increase in chemical inhomogeneity as the discharge time increases can be related directly to an increase in the volume fraction and size of Fe and LiF phases.

HR-EELS maps of FeF_2–C discharged for 42 h

A STEM image and corresponding EELS intensity maps of FeF_2–C electrode discharged for 42 h are shown in Fig. 8. The Fe–L_3 intensity map, and the Fe L_3/L_2 white line intensity ratio are displayed in Fig. 8b, c respectively. The F–K intensity map and the fluorine to iron ratio map (F–K divided by Fe–L_3) are shown in Fig. 8d, e respectively. Figure 5f represents individual EELS spectra extracted from marked areas in the F–K/Fe–L_3 ratio map in Fig. 8e.

The elemental intensity maps of Fe and F show that this sample, as expected, exhibit chemical inhomogeneity. Higher F intensities were observed at the edges while interior regions have lower F content or even nanodomains depleted of fluorine. Two representative EELS spectra taken from areas with large variation in F are shown in Fig. 8f. The spectra, which has been collected near the center (marked 1) shows a signal from Fe only, while the second spectra (marked 2) shows a significant amount of F in addition to Fe. The spectra which displays signal from iron only suggest that these regions have completely transformed into metallic iron ($FeF_2 \rightarrow Fe + LiF$). This can also be confirmed from our measured energy position of Fe–L_3 of 708.5 eV and from the low Fe L_3/L_2 ratio ($\sim$3.9) indicating of metallic Fe^0 as shown in our previous study (Cosandey et al. 2005; Cosandey et al. 2006). The F-signal depicted in curve *f*1 with small post peak is another indication that F is combined with Li to form LiF as mentioned earlier in the phase identification section.

HR-EELS maps of the fully discharged FeF_2–C electrode

The fully discharged electrode (56 h) has also been analyzed using selected area electron diffraction (SAED), Fig. 9, and EELS compositional mapping, Fig. 10. Analysis of the *d*-spacings of the indexed SAED pattern confirms the presence of mixed Fe and LiF phases. In addition, there is a weak intensity corresponding to (110) reflection of the FeF_2 phase (< 10 %), which is an indication of a trace of unreacted (retained) FeF_2 material. In order to reveal the chemical composition and elemental distribution, EELS compositional mapping were collected from the fully discharged sample. A representative STEM image is displayed in Fig. 10a. The Fe–L_3 intensity map and fluorine to iron (F–K divided by the Fe–L_3) intensity map ratio are shown in Fig. 10b, c respectively. The Li–K/Fe–L_3 intensity map ratio is displayed in Fig. 10d.

The F–K/Fe–L_3 intensity map shows a higher and relatively uniform F/Fe relative intensity at the core surrounded by strong Fe signal, which appeared in dark

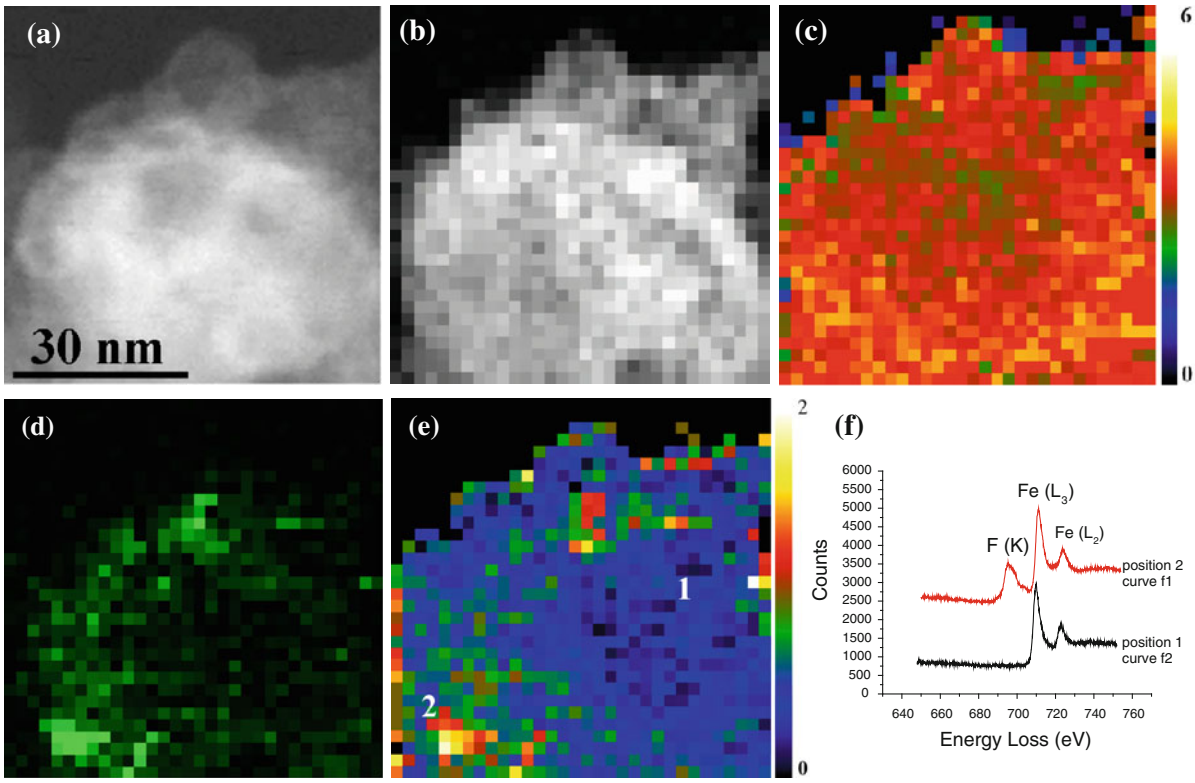

Fig. 8 EELS compositional maps of the 42 h discharged electrode. **a** STEM image, **b** Fe L_3 intensity map, **c** Fe L_3/L_2 intensity map ratio, **d** F–K intensity map, **e** F–K/Fe–L_3 intensity map ratio, **f** EELS spectra taken from positions marked *1* and *2* in **e** showing phase separation with high F and Fe (position 1) and only Fe signal (position 2) (each map is 64 by 64 nm^2)

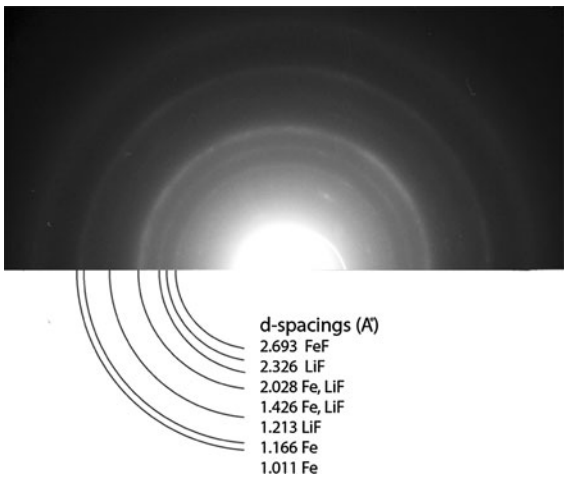

Fig. 9 An indexed selected area electron diffraction (SAED) pattern from the fully discharged FeF_2–C electrode, which confirms the decomposition of FeF_2 into LiF and Fe upon discharging

blue color. Individual spectra from various regions were also collected from this sample and a typical core-loss and low-loss spectra are presented in Fig. 10d, e respectively. The spectra from a standard LiF sample (Ahn and Krivanek 1983; Saifullah et al. 1999; Cosandey et al. 2005; Cosandey et al. 2006) is also displayed in Fig. 10e. The results form this sample reveal that most of the fluorine is combined as LiF as can be seen from the similar F edge features in both spectra. In the low-loss region (Fig. 10f), the Li–K edge is located at ~62 eV with a second peak located at ~68 eV. An energy window, which includes both edges (15 eV), was utilized to extract lithium signal from low-loss spectra with best intensity, Fig. 10d. The first peak which can be seen before the Li–K edge at around 58 eV is the onset of the $Fe_{M2,3}$ signal. By comparing Li map with F map it is very clear that there is a strong correlation between both maps, which is an indication of the formation of LiF nanodomains.

Discussion

Despite the beam sensitivity of FeF_2–C, EELS elemental maps have been obtained with a 2 nm de-focused

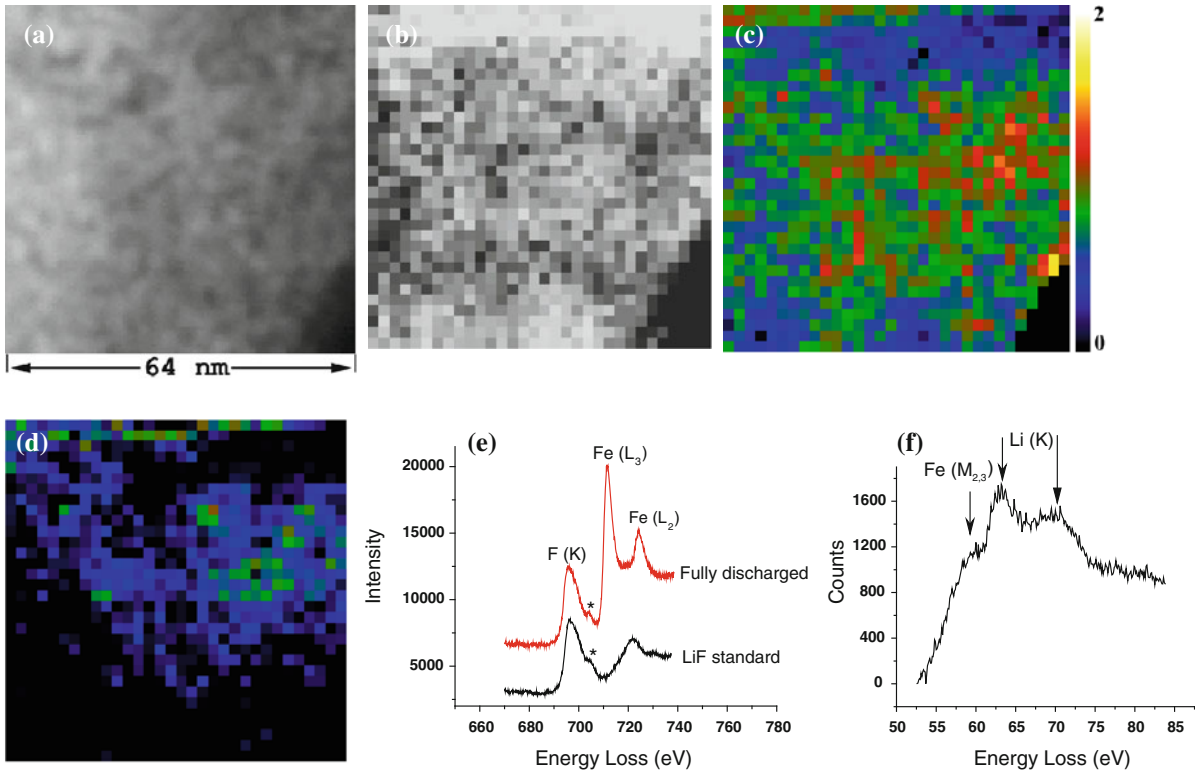

Fig. 10 EELS compositional maps of the fully discharged FeF_2–C nancomposite electrode. **a** STEM image, **b** Fe–L_3 intensity map, **c** F–K/Fe L_3 intensity map ratio, **d** Li–K/Fe–L_3 intensity map ratio, **e** core-loss signal with F–K and Fe–$L_{2,3}$ edges and, **f** low-loss spectra corresponding to Fig. 5e with Fe–$M_{2,3}$ and Li–K signal (each map is 64 by 64 nm^2)

probe and a dose of 3.8 10^4 C/cm^2. The results obtained from elemental maps show that upon discharge, there is a gradual transformation of FeF_2–C positive electrode into LiF and Fe, Fig. 11. The EELS spectrum imaging analysis presented here were capable of providing information on Fe, F, and Li signals. Although, the Li–K edge signal was in close proximity with the Fe–$M_{2,3}$ edge and also located too close to the Plasmon peaks, Li–K maps can still be obtained. In addition, low-loss spectra from individual spots were also frequently collected to check qualitatively for the presence of Li–K and Fe–$M_{2,3}$ signals allowing clear differentiation between F signal in LiF from unreacted F in FeF_2.

The gradual transformation of the FeF_2–C electrode upon lithiation (discharging) is displayed schematically in Fig. 11. The corresponding F/Fe ratio maps from this study are also included for comparison. Before discharging, a nearly homogenous FeF_2 nanocomposite is present in a conductive carbon matrix. The F/Fe spectrum image also shows an almost uniform intensity. During discharging, gradual phase transformation of FeF_2–C nanocomposite electrode into LiF and Fe is initiated upon reaction with Li. This process can be observed from the spectrum images of the sample discharged for 42 h showing a shrinkage of the $FeFe_2$ phase at the expenses of the LiF and Fe phases, Fig. 11. The corresponding F/Fe ratio spectrum image, also shows regions with pure Fe surrounded with LiF and FeF_2 regions.

The fluorine and F/Fe–L_3 relative intensity maps and line intensity profiles from electrode materials discharged at 20, 42, and 56 h (fully discharged) exhibits chemical inhomogeneities. For instance, the sample discharged for 20 h showed partial transformation with small compositional variations. However, increasing the discharge time to 42 h has resulted in chemical inhomogeneity and phase segregation on larger scale. This can be observed from the F and Fe line intensity profiles shown in Fig. 7, where the sample discharged for 20 h exhibits modulation with period of about 5 nm, which increases to about 10 nm in case of 42 h discharge. Chemical inhomogeneity in the fully discharged sample is in the range of 16 nm. This probably is an indication that under these reaction conditions the maximum domains will be no larger

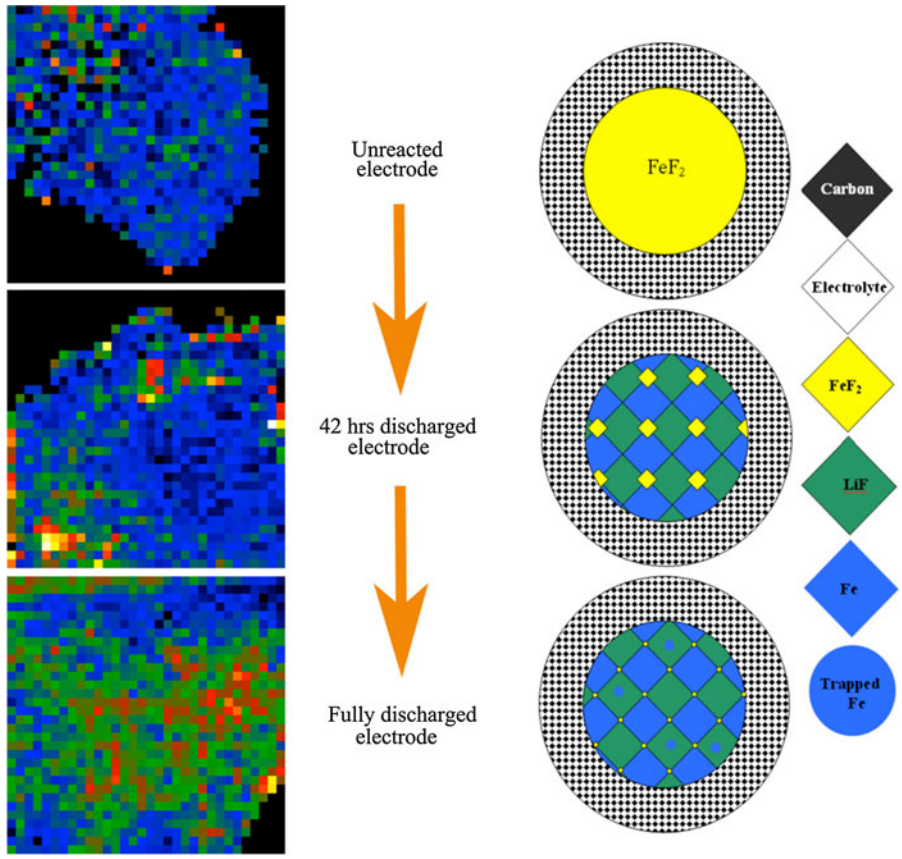

Fig. 11 Schematic with corresponding high-resolution EELS maps showing gradual transformation of the FeF_2 electrode into LiF and Fe upon discharging. Each map is 64 by 64 nm^2

than 16 nm due to diffusion kinetics. However, detailed experiments with higher spatial resolution are needed to confirm this observation. A recent in situ TEM study (Wang et al. 2011, Wang et al. 2012) confirms the modulation structure at the nanoscale.

When the FeF_2–C nanocoposite is fully discharged, the cathode material at this stage is fully decomposed into LiF and Fe phases as expected from the chemical reaction with Li (Eq. 1) and confirmed recently by other researchers (Rangan et al. 2012). The SAED, Fig. 9, and EELS results displayed in Fig. 10a–d confirm the presence of LiF and F phases. Detailed analysis of EELS maps combined with individual spectra from core-loss and low-loss regions, as typically shown in Fig. 10d–e, confirm that almost all the F in this sample is presented as LiF.

Conclusions

EELS spectrum imaging has been used to investigate a newly developed FeF_2–C nanocomposite used as positive electrode material for Li–ion batteries. Electrochemical data have shown that this new cathode material reacts with Li through a fully reversible process. In this study, EELS compositional as well as valence maps were used to investigate chemical inhomogeneity that accompanied the lithiation (discharged) process. Selected samples at different discharge values showed a decomposition of the FeF_2 into Fe and LiF upon reaction with Li ions. The FeF_2–C nanocomposite electrode material is highly beam sensitive to electron beam and about 2 % of the fluorine content was lost by radiation during the analysis. Nevertheless, this study was able to provide spectrum imaging of Fe, F, and Li, which allow deep insight regarding electrochemical reactions. In addition, this study is the first attempt to analyze iron fluoride materials using EELS mapping and the results show promise with sufficient resolution to reveal changes occurring during various electrodes discharged times. Atomic scale compositional mapping in electron beam-sensitive materials will be possible with minimum radiation damage and enough detectability.

Acknowledgments This project was supported by the US government. Research at the ORNL SHaRE User Facility was supported by the Office of Basic Energy Sciences, U.S. Department of Energy under contract DE-AC05-00OR22725 with UT-Battelle, LLC, and also formerly through the ShaRE Program under contract DE-AC05-76OR00033 with Oak Ridge Associated Universities.

References

Ahn CC, Krivanek OL (1983) EELS atlas. Gatan Inc

Amatucci GG, Tarascon JM, Klein LC (1996) CoO_2 the end member of the $LixCoO_2$ solid solution. J Electrochem Soc 143(3):1114–1123

Arai H, Okada S, Sakurai Y, Yamaki J (1997) Cathode performance and voltage estimation of metal trihalides. J Power Sources 68:716–719

Badway F, Pereira N, Cosandey F, Amatucci GG (2003a) Carbon-metal fluoride nanocomposites, structure and electrochemistry of FeF_3. J Electrochem Soc 150:A1209–A1218

Badway F, Cosandey F, Pereira N, Amatucci GG (2003b) Carbon metal fluoride nanocomposites high-capacity reversible metal fluoride conversion materials as rechargeable positive electrodes for Li batteries. J Electrochem Soc 150:A1318–A1327

Badway F, Pereira N, Cosandey F, Amatucci GG (2003c) Carbon metal fluoride nanocomposites high-capacity reversible metal fluoride conversion materials as rechargeable positive electrodes for Li batteries. Mater Res Soc Symp Proc 756:207

Chen Z, Li Z, Dahn JR (2002) Staging phase transitions in $LixCoO_2$. J Electrochem Soc 149(12):A1604–A1609

Chen JS, Zhang Y, Lou XW (2011) One-pot synthesis of uniform Fe_3O_4 nanospheres with carbon matrix support for improved lithium storage capabilities. ACS Appl Mater Interfaces 3(9):3276–3279

Cosandey F, Al-Sharab JF, Badway F, Amatucci GG (2005) HRTEM imaging and EELS spectroscopy of lithiation process in FeFx:C nanocomposites, vol 161. Transactions of the American Ceramic Society, Westerville, pp 111–119

Cosandey F, Al-Sharab JF, Amatucci GG, Stadelmann P (2006) EELS spectroscopy of FeFx/C nanocomposite electrodes used in Li-ion batteries. Microsc Microanal 13(2):87

Dupin JC, Gonbeau D, Martin-Litas I, Binatier P, Levasseur A (2001) Lithium intercatlation/deintercalatin in transions metaql oxisdes inbestigated by x-ray photoelectron spectroscopy. J Electron Spectrosc Relat Phenom 120:55–65

Egerton RF (1996) Electron Energy-Loss spectroscopy in the electron microscope. Plenum Press, New York

Gabrisch H, Yazami R, Fultz B (2005) Hexagonal to cubic spinel transformation in lithiated cobalt oxide (TEM investigation). J Electrochem Soc 151(6):A891–A897

Garvie LAJ, Craven AJ, Braydson R (1994) Use of electron-energy loss near-edge fine structure in the study of minerals. Am Mineral 79:411–425

Kosova NV, Kaichev VV, Bukhtyarov VI, Kellerman DG, Devyatkia ET, Larin TV (2003) Electronic state of cobalt and oxygen ions in stoichiometric and nonstoichiometric $Li1 + xCoO_2$ before and after delithiation according to XPS and DRS. J Power Sources 119–121:669–673

Markovsky B, Nimberger A, Talyosef Y, Rodkin A, Belostotskii AM, Salitra G, Aurbach D, Kim H-J (2004) On the influence or additives in electrolyte solution on the electrochemical behavior of carbon/$LiCoO_2$ cell at elevated temperatures. J Power Sources 136:296–302

Nazri G-A (ed) (2003) Lithium batteries science and technology, 1st edn. Springer, New York, p 12

Nazri GA (ed) (2004) Lithium batteries science and technology, 1st edn. Springer, New York, p 58

Plitz FB, Al-Sharab JF, DuPasquier A, Cosandey F, Amatucci GG (2005) Structure and electrochemistry of carbon-metal fluoride nanocomposites fabricated by solid-state redox conversion reaction. J Electrochem Soc 152(2):A307–A315

Poizot P, Laruelle S, Grugeon S, Dupont L, Tarascon JM (2000) Nano-sized transition-metal oxides as negative-electrode materials for lithium-ion batteries. Nature 407:496

Rangan S, Thorpe R, Bartynski RA, Sina M, Cosandey F, Celik O, Mastrogiovanni DDT (2012) Conversion reaction of FeF_2, thin films upon exposure to atomic lithium. J Phys Chem C 116:10498–10503. doi:10.1021/jp300669d

Reimer L (1995) Energy-filtered transmission electron microscopy. Springer, Berlin

Saifullah MSM, Botton GA, Boothroyd CB, Humphrey CJ (1999) Energy loss spectroscopy studies of the amorphous to crystalline transition in FeF_3. J Appl Phys 86(5):2499–2504

Shao-Horn Y, Levasseur S, Weill F, Delmas C (2003) Probing lithium and vacancy ordering in O_3 layered $LixCo_2(x \sim 0.5)$ an electron diffraction study. J Electrochem Soc 150(3):A366–A373

Wan H, Jang Y-I, Huang B, Sasoway DR, Chiang Y-M (1999) TEM observation of electrochemical cycling—induced damage and disorder in $LiCoO_2$ cathodes for rechargeable lithium batteries. J Electrochem Soc 146(2):473–480

Wang F, Robert R, Chernova NA et al (2011) Conversion reaction mechanisms in lithium ion batteries: study of the binary metal fluoride electrodes. J Am Chem Soc 133(46):18828–18836. doi:10.1021/ja206268a

Wang F, Yu H-C, Chen M-H, Wu L, Pereira N, Thornton K, Ven A, Zhu Y, Amatucci Glenn G, Graetz J (2012) Tracking lithium transport and electrochemical reactions in nanoparticles. Nature Commun 3:1201. doi:10.1038/ncomms2185